

Star Log-extended eMulation: a method for efficient computation of the Tolman-Oppenheimer-Volkoff equations

Sudhanva Lalit ^{1,*} Alexandra C. Semposki ^{2,†} and Joshua M. Maldonado ^{2,‡}

¹*Facility for Rare Isotope Beams, Michigan State University, East Lansing, MI 48824, USA*

²*Department of Physics and Astronomy, and Institute of Nuclear and Particle Physics, Ohio University, Athens, OH 45701, USA*

(Dated: November 19, 2024)

We emulate the Tolman-Oppenheimer-Volkoff (TOV) equations, including tidal deformability, for neutron stars using a novel hybrid method based upon the Dynamic Mode Decomposition (DMD) for the first time. This new method, which we call Star Log-extended eMulation (SLM), utilizes the underlying logarithmic behavior of the differential equations to enable accurate emulation of the nonlinear system. We show predictions for well-known phenomenological equations of state (EOS) with fixed parameters and with a freely-varying parametric Quarkyonic EOS. Our results produce a significant computational speed-up of $\approx 3 \times 10^4$ compared to high fidelity (HF) calculations using standard Runge-Kutta methods, providing an efficient emulator for the numerous TOV evaluations required by multi-messenger astrophysical frameworks that infer constraints on the EOS from neutron star mergers. The ability of the SLM algorithm to learn a mapping between parameters of the EOS and subsequent neutron star properties also opens up potential extensions for assisting in computationally prohibitive uncertainty quantification (UQ) for any type of EOS. The source code for the methods developed in this work will be openly available in a public GitHub repository for community modification and use.

Introduction.—The advent of multi-messenger astronomy, accelerated by LIGO’s gravitational wave measurements [1–3] and NICER’s pulsar observations [4–8], has coincided perfectly with advances in Bayesian uncertainty quantification (UQ) in nuclear physics [9, 10] and the FRIB era of experiment [11]. These three complementary approaches enable a refined understanding of the strong interaction, which governs matter from finite nuclei to dense, stellar compact objects, e.g., neutron stars. These intriguing astrophysical laboratories provide us with critical insights on extreme matter not found terrestrially. However, the lack of direct probes into the interior composition of neutron star cores indicates that we must rely on the combination of data from neutron-star observations and binary mergers, nuclear experiment [12, 13], and the construction of state-of-the-art nuclear potentials to infer the equation of state (EOS) of the full system [14–16]. This description of a neutron star through the state variables, e.g., pressure, number density, and energy density, is propagated through the Tolman-Oppenheimer-Volkoff (TOV) equations [17, 18] to determine the corresponding mass and radius of the star. Future gravitational wave (GW) measurements, as well as data from NICER and Cosmic Explorer, will provide more constraints on this mass-radius relationship, including other important properties such as tidal deformability [19–23], which will, in turn, allow us to place tighter constraints on the EOS of neutron-rich matter.

This multi-messenger era of astrophysics has led to the need for more efficient calculations of the TOV equations due to their use in large-scale frameworks, e.g., LIGO’s GW inference framework [24–26], where thousands of solutions can be required for reliable UQ of

the mass-radius posterior. The precision era of nuclear physics [16, 27–31] has also led to the use of smaller-scale Bayesian frameworks that require sampling of the EOS and the computation of posteriors for neutron star properties [16, 30, 32, 33], and also rely on numerous solutions to the TOV equations. To perform these calculations efficiently, the computational burden of solving the TOV equations, especially when tidal deformability is included, must be overcome. An approach already being employed in nuclear physics is the design and use of sophisticated emulators to reduce computational time and resources. Recent efforts in constructing model-intrusive, projection-based emulators have produced remarkable results in nuclear scattering [34–38], and model-extrusive emulators such as Gaussian processes (GPs) have long been used successfully in nuclear astrophysics [30, 39].

In this Letter, we introduce a novel emulation strategy inspired by the well-known Dynamic Mode Decomposition (DMD) method used in analyses of time dynamics [40–42], which we call Star Log-extended eMulation (SLM). Currently available DMD libraries [43] are incapable of handling the nonlinearity of the TOV equations; hence, this work develops and demonstrates the accuracy and computational speed-up of an emulator that is able to overcome this hurdle. We apply two state-of-the-art SLM emulators to the TOV equations, including tidal deformability, for the first time. We begin by benchmarking the emulator against high fidelity solutions to these equations. We then employ two versions of this emulation strategy: one to nonparametric, e.g., tabular EOSs, and another, designed for parametric EOSs, to a two-parameter Quarkyonic EOS. The latter learns a mapping between EOS parameters and previously mentioned neu-

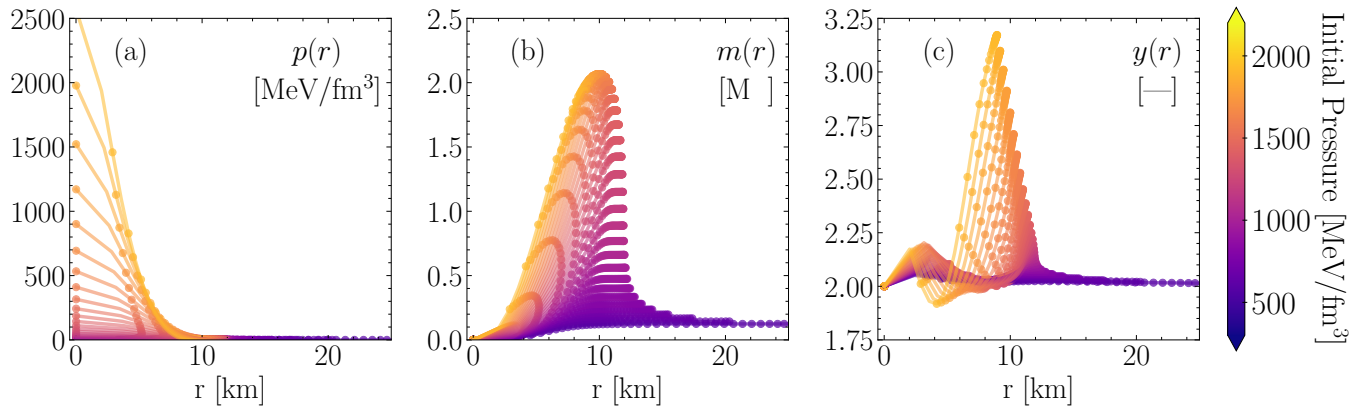


FIG. 1. Solutions to the TOV and tidal deformability coupled differential equations (solid curves), for given initial conditions, and their SLM fits (dotted curves). The results shown are for the SLy4 tabular EOS [44], and highlight the ability of the SLM routine to capture the underlying structure of the nonlinear differential equations.

tron star properties, a necessary feature for the Bayesian calibration of other phenomenological EOSs with freely varying parameters. Our emulators, along with the code to produce the results shown in this Letter, will be publicly available for community use [45].

Neutron star properties.—Macroscopic properties of neutron stars, including mass and radius, tidal deformabilities, and moment of inertia, can be determined by solving the TOV equations simultaneously with appropriate differential equations corresponding to each additional desired quantity. We use the scaled versions of the TOV equations [46] and scale the differential equation for tidal deformability [20–22] in a similar fashion.

The resulting scaled equations are

$$\frac{dp}{dx} = \frac{1}{2} \frac{(\varepsilon(x) + p(x)) (m(x) + 3x^3 p(x))}{x^2 (1 - m(x)/x)} \quad (1)$$

$$\frac{dm}{dx} = 3x^2 \varepsilon(x) \quad (2)$$

$$\frac{dy}{dx} = -\frac{y(x)^2}{x} - \frac{F(x)y(x)}{x} - \frac{Q(x)}{x} \quad (3)$$

with

$$F(x) = \frac{1 - \frac{3}{2}(\varepsilon(x) - p(x))}{1 - \frac{m(x)}{x}}$$

and

$$Q(x) = \frac{\frac{3}{2}x^2}{\left(1 - \frac{m(x)}{x}\right)} \left[5\varepsilon(x) + 9p(x) + \frac{\varepsilon(x) + p(x)}{c_s^2(x)} - \frac{4}{x^2} \right] - \left(\frac{m(x)/x + 3x^2 p(x)}{\left(1 - \frac{m(x)}{x}\right)} \right)^2,$$

where $p(x)$, $\varepsilon(x)$, $m(x)$ and $c_s(x)$ are the scaled dimensionless pressure, energy density, mass and the speed-of-sound functions respectively, while $y(x)$ is the scaled

solution to the tidal equation. As can be seen from equations (1)–(3), the dense matter EOS is the essential input to this system, as well as the initial conditions to ensure physical conditions, e.g., $p(x) \rightarrow 0$ at the edge of the star. We solve these equations simultaneously to obtain masses, radii, and tidal deformabilities, Λ , of neutron stars using a high-fidelity (HF) fourth order Runge-Kutta (RK4) solver. We also construct the dimensionless coefficient, k_2 , known as the Love number [22].

As input to the TOV solver, we have chosen EOSs that can obtain a maximum mass of greater than $2M_\odot$, possess different sets of underlying parameters, and enable us to test our algorithm on a variety of masses and radii, as well as various structures of the Love number curve, $k_2(R)$. Our HF solutions for maximum masses and corresponding radii are presented in Table I, and are consistent with the results in the compOSE database [44].

Star Log-extended eMulation (SLM).—Existing model-extrusive emulators, such as DMDs, are appealing to consider for use in emulating the TOV equations. DMD-based emulators are generally applicable to problems that have either polynomial nonlinearities or can be expressed as an eigenvalue problem [34, 35, 38, 54], and are used extensively for emulation of various time-dependent systems [55–58]. DMDs can also be used to solve nonlinear time-independent problems as has been shown in a recent work [59]. However, they possess a significant drawback—current DMD algorithms suffer from the inability to capture the more complex nonlinear dynamics of the coupled TOV system. To overcome this limitation, we design a new method that originates from a modification of the DMD emulator [41]. In the standard DMD algorithm, one seeks a family of surrogate equations for a given system of coupled, time-dependent differential equations. In our case, we solve a similar system of equa-

EOS	HF		SLM		Error (%)		Time (s)	
	Max. Mass [M_{\odot}]	Radius [km]	Max. Mass [M_{\odot}]	Radius [km]	Max. Mass	Radius	HF	SLM
Tabular EOS								
SLy4	2.067	10.033	2.068	10.033	0.02	0.00	9.218	2.135×10^{-4}
APR	2.193	9.979	2.194	9.982	0.05	0.03	9.237	2.149×10^{-4}
FSU Garnet	2.054	10.998	2.068	11.000	0.66	0.02	9.226	2.319×10^{-4}
BL	2.083	10.194	2.085	10.204	0.10	0.11	9.246	2.099×10^{-4}
DS-CMF-5	2.023	11.896	2.026	11.647	0.17	2.09	9.228	2.215×10^{-4}
Quarkyonic EOS								
$\Lambda=300.00, \kappa=0.19$	2.947	14.763	2.917	14.666	1.00	0.66	9.286	3.822×10^{-4}
$\Lambda=352.63, \kappa=0.14$	2.653	12.512	2.675	12.561	0.83	0.39	9.299	4.051×10^{-4}
$\Lambda=405.26, \kappa=0.10$	2.441	11.199	2.441	11.063	0.40	1.21	9.234	4.361×10^{-4}
$\Lambda=447.37, \kappa=0.28$	2.294	10.462	2.294	10.463	0.01	0.01	9.292	4.261×10^{-4}
$\Lambda=500.00, \kappa=0.23$	2.226	10.180	2.221	10.177	0.22	0.03	9.156	3.898×10^{-4}

TABLE I. Comparisons of the high-fidelity and emulated maximum mass and corresponding radii for various EOSs selected from the compOSE database [44], as well as the same quantities computed for the Quarkyonic EOS [53] with various choices of parameters Λ and κ . The tabular EOSs are emulated using the SLM algorithm (see Fig. 2), whereas the Quarkyonic EOS is emulated through the pSLM algorithm (see Fig. 3). The remarkable efficiency achieved is seen in the large difference between the time spent computing the emulated and HF solutions (last two columns), leading to an average overall speed-up of 2.95×10^4 .

tions, which can be written as

$$\frac{\partial \mathbf{y}}{\partial r} = \mathcal{F}(\mathbf{y}(\mathbf{x}, r)), \quad (4)$$

where \mathcal{F} is a nonlinear operator that describes the governing equation of interest through a discretization of the phase space, i.e., snapshots at discrete values of r . Here r is the independent variable, e.g., scaled radius, while \mathbf{x} consists of other dependent variables such as ε . We seek the following surrogate system

$$\frac{d\mathbf{y}}{dr} = \hat{\mathbf{A}}\mathbf{y}, \quad (5)$$

which, in effect, assumes that the data collected was generated from linear dynamics and that the linear operator $\hat{\mathbf{A}}$ approximates these dynamics. The operator $\hat{\mathbf{A}}$, a finite approximation of the infinite dimensional *Koopman operator*, is learned in a data-driven fashion.

Due to the lack of time dependence in Eq. (4), it does not fall within the general category of problems to which DMD is directly applicable. Thus, in the DMD procedure, we replace the independent variable t with the linear index of the data in the training set, and include the independent variable r , e.g., the scaled radius, in the set of snapshots. We perform the DMD algorithm for the logarithm of the chosen snapshots, i.e., $\log r$, $\log p(r)$, $\log m(r)$ and $\log y(r)$, due to the logarithmic manifestation of the nonlinearities in the system. We employ the formalism of extended DMDs in Ref. [60] to modify the data to make it suitable for our calculations, e.g., by utilizing polynomial extensions of the general DMD algorithm (see the supplemental material [61] for more details). Instead of using the solutions to Eqs. (1)-(3) for the SLM routine, one can also consider the neutron star mass $M(R)$, radius R , central pressure

$P_{\text{central}}(R)$ and $k_2(R)$ (see Fig. 2) for the SLM algorithm and follow the same procedure above.

Parametric-SLM.—The parametric-SLM (pSLM) method is similar to that of the reduced Eigen-Pair Interpolation method (rEPI) from [57], using our modified snapshots. However, instead of using a point-wise Lagrange interpolation, we use a recently developed technique based on the Greedy Recombination Interpolation Method (GRIM) for Banach spaces (B-GRIM) [62] to interpolate within the parameter space. B-GRIM for interpolation is generally better for high-dimensional spaces where residual minimization in Banach spaces is effective. This is especially true when dealing with noisy data or requiring iterative improvement of the solution, whereas Lagrange interpolation is unstable in such cases. In this method, the objective is to construct an interpolant that minimizes the norm (ℓ^1) in that space. In the greedy recombination method, the algorithm iteratively selects basis elements to improve the interpolation, minimizing the error at each step.

In our case, pSLM allows us to find the relation between the parameters of the EOS to the neutron star properties described by the solutions to the TOV equations, through a modification to Eq. (5),

$$\frac{d\mathbf{y}^{\theta}}{dr} = \hat{\mathbf{A}}(\boldsymbol{\theta})\mathbf{y}^{\theta}, \quad (6)$$

where $\boldsymbol{\theta}$ is a vector of parameters corresponding to the prediction set. Thus, pSLM can be employed to predict at parameters that have not been used to train the emulator (see the supplemental material [61] for the full pSLM algorithm).

Results.—Fig. 1 shows the solutions to Eqs. (1)-(3) as functions of radius r and the output from the SLM algorithm for each quantity, respectively. The emulator is

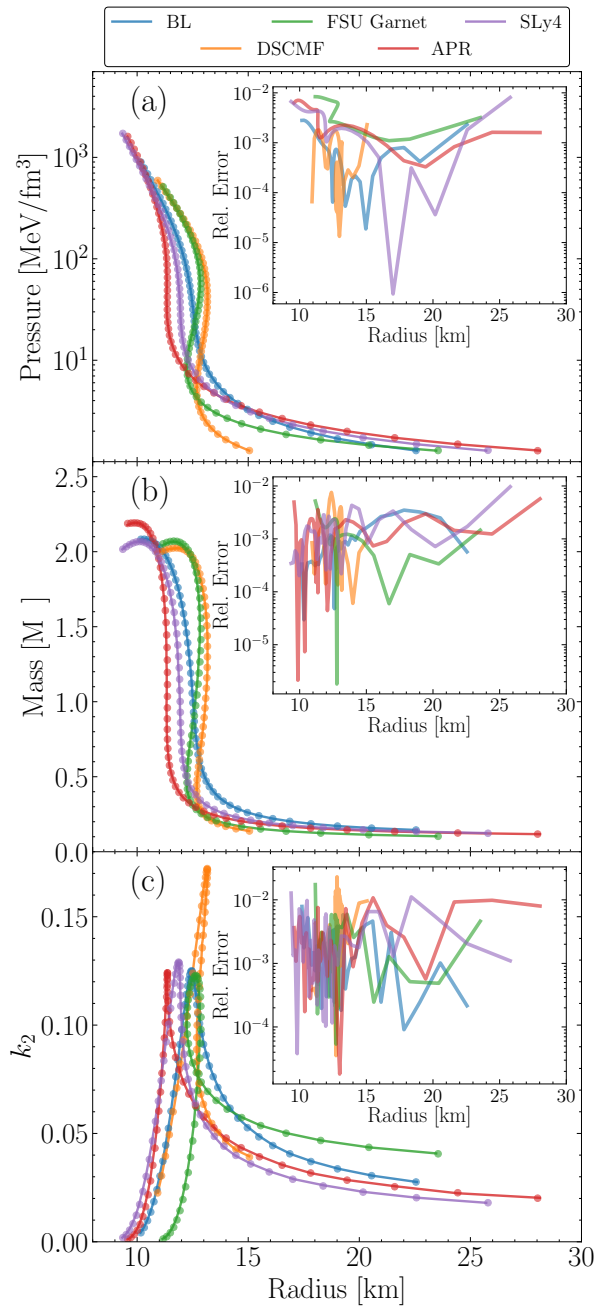


FIG. 2. (a) Central pressure, (b) mass, and (c) dimensionless Love number k_2 as functions of radius. These properties are calculated for five tabular EOSs [47–52]. The solid lines are the HF solutions, while the dots correspond to the SLM results. The inset shows the relative error between the HF and SLM results.

able to recover the solutions from the HF solver, allowing for accurate predictions between HF solutions. Hence, SLM only needs a few solutions of each quantity to reliably reconstruct the HF results. Fig. 2 then shows SLM applied to the HF solutions of $M - R$, $P_{\text{central}} - R$, and $k_2 - R$ curves for the chosen tabular EOSs and the respective relative errors between the HF and emulated results,

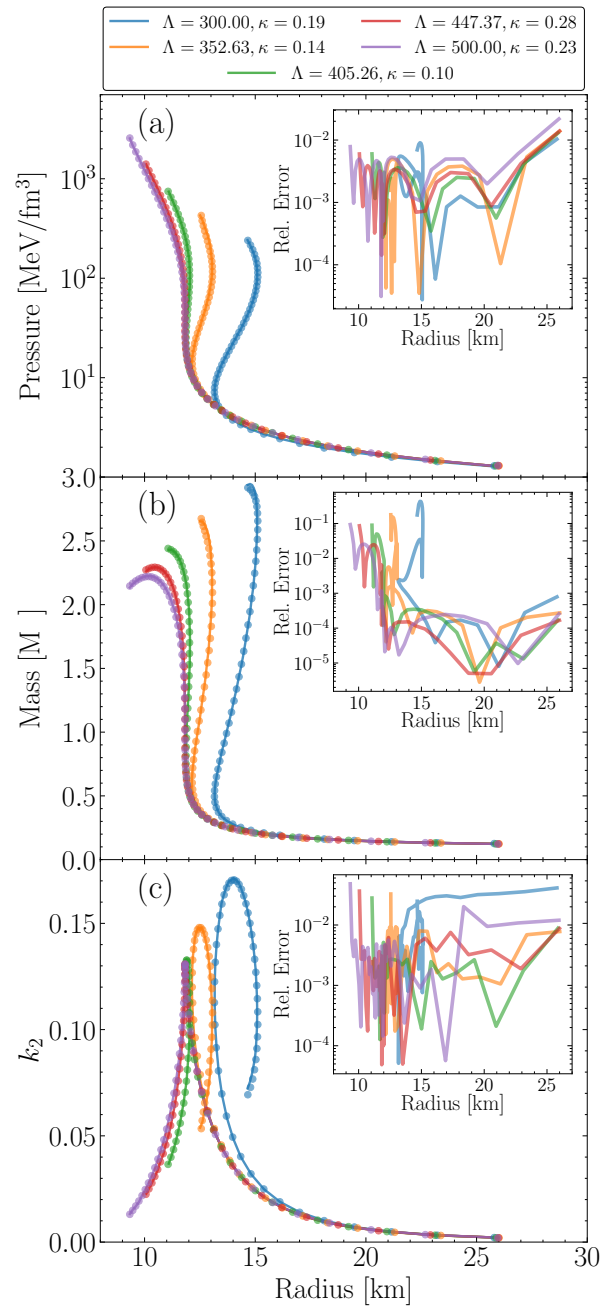


FIG. 3. (a) Central pressure, (b) mass, and (c) dimensionless Love number k_2 as function of radius for the Quarkyonic EOS [53] using pSLM, with varying parameters Λ and κ . The result shown here is the prediction for a given test parameter set that has not been used to train the emulator. The dots indicate SLM results, while the solid lines are the TOV results.

found to be approximately 1×10^{-3} . With an average speed of about 2.2×10^{-4} seconds, compared to the HF average speed of ≈ 9.2 seconds, the SLM routine is shown to be remarkably efficient. This proof-of-principle calculation also indicates that SLM can be used to accurately recover the structure of each curve through prediction

between HF solutions corresponding to a given EOS. Table I shows the numerical results for the maximum masses and corresponding radii calculated from the HF solver for these EOSs, the same quantities using the SLM algorithm, and the subsequent percent error between the HF and emulated calculations. All errors are $\leq 1\%$ for the maximum mass, and $< 3\%$ for the corresponding radii.

We use the Quarkyonic EOS to test our pSLM algorithm, varying parameters Λ and κ over a range of 300 – 500 MeV and 0.1 – 0.3, respectively. The training set is composed of 15 datasets consisting of radii, central pressures, masses and Love numbers. Using pSLM we predict the curves for test parameter sets as shown in Fig. 3, which were not used to train the emulator. The maximum mass and radius results from the HF solver and the pSLM emulator, as well as the percent error and speed of the calculation, are also recorded in Table I. The average speed for the pSLM emulator is $\approx 4.1 \times 10^{-4}$ seconds, yielding an overall speed up of $\approx 4.5 \times 10^4$ over the HF method. All percent errors are $\leq 1\%$ for all maximum masses and radii.

Summary and outlook.—In this work, we introduced SLM as a new method to emulate, specifically, the TOV equations, including tidal deformabilities. We employed SLM to emulate $M - R$ curves from tabular EOSs, such as the well-known SLy4 and APR EOSs. We then employed a parametric version of SLM, pSLM, to emulate EOSs that possess an arbitrary number of parameters. In particular, we focused on the Quarkyonic EOS. The results from these emulators agree well with HF RK4 evaluations of the TOV equations. We gain an average computational speed-up of $\sim 3 \times 10^4$ across both types of EOSs considered; hence, both SLM algorithms present highly efficient emulators for large-scale computations of the TOV equations in scenarios such as those presented by multi-messenger astrophysical inference frameworks. This emulation strategy will help to reduce the bottleneck that the TOV equations present in such calculations, without sacrificing necessary accuracy.

A straightforward application of this work is to EOSs that possess multiple parameters, e.g., Skyrme energy density functionals [49, 63–65] and other mean field-based approaches [51]. The algorithm is not limited to small parameter sets, and as such can be easily generalized. More broadly, the SLM algorithm works well for problems that possess logarithmic dependence in the solutions. Hence, our work can be naturally extended in future to problems that share this trait, e.g., density functionals with non-affine parameter dependence. Additionally, extensions to EOSs possessing various types of phase transitions is an exciting avenue of research we are currently pursuing. To help other researchers utilize and build upon our work, the code pertaining to our SLM algorithm and the generation of the results in this Letter, as well as tutorials to assist new users, will be published

in a public GitHub repository for the use of the scientific community [45].

We thank Jérôme Margueron for a careful review of our manuscript, Xilin Zhang for engaging discussions, Amy L. Anderson for providing the FSUGarnet data, and ComPOSE (<https://compose.obspm.fr>) for providing all other tabular EOS datasets. A.C.S. thanks the Facility for Rare Isotope Beams for their hospitality and encouragement during the completion of this work. This work is supported by the CSSI program, Award OAC-2004601 (BAND collaboration [66]) (A.C.S.), and the U.S. Department of Energy, Office of Science, Nuclear Physics, under Award DE-SC0023688 (S.L.), Award DE-FG02-93-40756 (A.C.S.) and Award DE-SC0024233 (STREAMLINE collaboration) (J.M.M.).

* lalit@frib.msu.edu

† as727414@ohio.edu

‡ jm998521@ohio.edu

- [1] B. P. Abbott *et al.* (LIGO Scientific, Virgo), *Phys. Rev. Lett.* **119**, 161101 (2017), arXiv:1710.05832 [gr-qc].
- [2] B. P. Abbott *et al.* (LIGO Scientific, Virgo), *Phys. Rev. Lett.* **121**, 161101 (2018), arXiv:1805.11581 [gr-qc].
- [3] B. P. Abbott *et al.* (LIGO Scientific, Virgo), *Astrophys. J. Lett.* **892**, L3 (2020), arXiv:2001.01761 [astro-ph.HE].
- [4] M. C. Miller *et al.*, *Astrophys. J. Lett.* **887**, L24 (2019), arXiv:1912.05705 [astro-ph.HE].
- [5] M. C. Miller *et al.*, *Astrophys. J. Lett.* **918**, L28 (2021), arXiv:2105.06979.
- [6] T. E. Riley *et al.*, *Astrophys. J. Lett.* **887**, L21 (2019), arXiv:1912.05702 [astro-ph.HE].
- [7] T. E. Riley *et al.*, *Astrophys. J. Lett.* **918**, L27 (2021), arXiv:2105.06980.
- [8] D. Choudhury *et al.*, *Astrophys. J. Lett.* **971**, L20 (2024), arXiv:2407.06789 [astro-ph.HE].
- [9] D. R. Phillips, R. J. Furnstahl, U. Heinz, T. Maiti, W. Nazarewicz, F. M. Nunes, M. Plumlee, M. T. Prato, S. Pratt, F. G. Viens, and S. M. Wild, *J. Phys. G* **48**, 072001 (2021), arXiv:2012.07704 [nucl-th].
- [10] J. A. Melendez, R. J. Furnstahl, D. R. Phillips, M. T. Prato, and S. Wesolowski, *Phys. Rev. C* **100**, 044001 (2019), arXiv:1904.10581.
- [11] B. A. Brown *et al.*, (2024), arXiv:2410.06144 [nucl-th].
- [12] A. Sorensen *et al.*, *Prog. Part. Nucl. Phys.* **134**, 104080 (2024), arXiv:2301.13253.
- [13] R. Kumar *et al.* (MUSES), (2023), arXiv:2303.17021.
- [14] C. Drischler, J. W. Holt, and C. Wellenhofer, *Annu. Rev. Nucl. Part. Sci.* **71**, 403 (2021), arXiv:2101.01709.
- [15] J. M. Lattimer, *Ann. Rev. Nucl. Part. Sci.* **71**, 433 (2021).
- [16] H. Koehn *et al.*, (2024), arXiv:2402.04172 [astro-ph.HE].
- [17] R. C. Tolman, *Physical Review* **55**, 364 (1939).
- [18] J. R. Oppenheimer and G. M. Volkoff, *Physical Review* **55**, 374 (1939).
- [19] K. S. Thorne and A. Campolattaro, “Non-Radial Pulsation of General-Relativistic Stellar Models. I. Analytic Analysis for $L \geq 2$,” (1967).
- [20] T. Hinderer, *Astrophys. J.* **677**, 1216 (2008), [Erratum: *Astrophys. J.* 697, 964 (2009)], arXiv:0711.2420 [astro-

- ph].
- [21] T. Hinderer, B. D. Lackey, R. N. Lang, and J. S. Read, *Phys. Rev. D* **81**, 123016 (2010), arXiv:0911.3535 [astro-ph.HE].
- [22] S. Postnikov, M. Prakash, and J. M. Lattimer, *Phys. Rev. D* **82**, 024016 (2010), arXiv:1004.5098 [astro-ph.SR].
- [23] C. C. Moustakidis, T. Gaitanos, C. Margaritis, and G. A. Lalazissis, *Bulg. J. Phys.* **44**, 093 (2017).
- [24] P. T. H. Pang *et al.*, *Nature Commun.* **14**, 8352 (2023), arXiv:2205.08513 [astro-ph.HE].
- [25] R. Abbott *et al.* (KAGRA, VIRGO, LIGO Scientific), *Phys. Rev. X* **13**, 011048 (2023), arXiv:2111.03634 [astro-ph.HE].
- [26] B. P. Abbott *et al.* (LIGO Scientific, Virgo), *Phys. Rev. Lett.* **119**, 161101 (2017), arXiv:1710.05832 [gr-qc].
- [27] C. Drischler, J. A. Melendez, R. J. Furnstahl, and D. R. Phillips, *Phys. Rev. C* **102**, 054315 (2020), arXiv:2004.07805 [nucl-th].
- [28] C. Drischler, R. J. Furnstahl, J. A. Melendez, and D. R. Phillips, *Phys. Rev. Lett.* **125**, 202702 (2020), arXiv:2004.07232 [nucl-th].
- [29] C. Drischler, S. Han, J. M. Lattimer, M. Prakash, S. Reddy, and T. Zhao, *Phys. Rev. C* **103**, 045808 (2021), arXiv:2009.06441 [nucl-th].
- [30] A. C. Semposki, C. Drischler, R. J. Furnstahl, J. A. Melendez, and D. R. Phillips, (2024), arXiv:2404.06323 [nucl-th].
- [31] B. Hu *et al.*, *Nature Phys.* **18**, 1196 (2022), arXiv:2112.01125 [nucl-th].
- [32] B. T. Reed, R. Somasundaram, S. De, C. L. Armstrong, P. Giuliani, C. Capano, D. A. Brown, and I. Tews, (2024), arXiv:2405.20558 [astro-ph.HE].
- [33] P. T. H. Pang, L. Sivertsen, R. Somasundaram, T. Dietrich, S. Sen, I. Tews, M. W. Coughlin, and C. Van Den Broeck, *Phys. Rev. C* **109**, 025807 (2024), arXiv:2308.15067 [nucl-th].
- [34] C. Drischler, J. A. Melendez, R. J. Furnstahl, A. J. Garcia, and X. Zhang, *Front. in Phys.* **10**, 1092931 (2022), arXiv:2212.04912 [nucl-th].
- [35] E. Bonilla, P. Giuliani, K. Godbey, and D. Lee, *Phys. Rev. C* **106**, 054322 (2022), arXiv:2203.05284 [nucl-th].
- [36] J. Maldonado, C. Drischler, and R. J. Furnstahl, “Greedy emulators for nuclear two-body scattering,” (2024), in preparation.
- [37] P. Giuliani, K. Godbey, E. Bonilla, F. Viens, and J. Piekarewicz, *Front. Phys.* **10** (2023), 10.3389/fphy.2022.1054524, arXiv:2209.13039.
- [38] D. Odell, P. Giuliani, K. Beyer, M. Catacora-Rios, M. Y. H. Chan, E. Bonilla, R. J. Furnstahl, K. Godbey, and F. M. Nunes, *Phys. Rev. C* **109**, 044612 (2024), arXiv:2312.12426 [physics.comp-ph].
- [39] R. Essick, I. Tews, P. Landry, S. Reddy, and D. E. Holz, *Phys. Rev. C* **102**, 055803 (2020), arXiv:2004.07744 [astro-ph.HE].
- [40] J. H. Tu, C. K. Rowley, D. M. Luchtenburg, S. L. Brunton, and J. N. Kutz, *Journal of Computational Dynamics* **1**, 391 (2014).
- [41] J. N. Kutz, S. L. Brunton, B. W. Brunton, and J. L. Proctor, *Dynamic Mode Decomposition* (Society for Industrial and Applied Mathematics, Philadelphia, PA, 2016) <https://epubs.siam.org/doi/pdf/10.1137/1.9781611974508>.
- [42] S. L. Brunton, M. Budišić, E. Kaiser, and J. N. Kutz, “Modern koopman theory for dynamical systems,” (2021), arXiv:2102.12086 [math.DS].
- [43] N. Demo, M. Tezzele, and G. Rozza, *Journal of Open Source Software* **3**, 530 (2018).
- [44] S. Typel *et al.* (CompOSE Core Team), *Eur. Phys. J. A* **58**, 221 (2022), arXiv:2203.03209 [astro-ph.HE].
- [45] S. Lalit, A. C. Semposki, and J. M. Maldonado (2024) <https://github.com/asempski/SLM>.
- [46] J. Piekarewicz, “Neutron star matter equation of state,” in *Handbook of Supernovae*, edited by A. W. Alsabti and P. Murdin (Springer International Publishing, Cham, 2017) pp. 1075–1094.
- [47] I. Bombaci and D. Logoteta, *Astron. Astrophys.* **609**, A128 (2018), arXiv:1805.11846 [astro-ph.HE].
- [48] W.-C. Chen and J. Piekarewicz, *Phys. Lett. B* **748**, 284 (2015), arXiv:1412.7870 [nucl-th].
- [49] E. Chabanat, P. Bonche, P. Haensel, J. Meyer, and R. Schaeffer, *Nucl. Phys. A* **627**, 710 (1997).
- [50] V. Dexheimer, R. O. Gomes, T. Klähn, S. Han, and M. Salinas, *Phys. Rev. C* **103**, 025808 (2021).
- [51] V. Dexheimer and S. Schramm, *Astrophys. J.* **683**, 943 (2008), arXiv:0802.1999 [astro-ph].
- [52] A. Akmal, V. R. Pandharipande, and D. G. Ravenhall, *Phys. Rev. C* **58**, 1804 (1998).
- [53] L. McLerran and S. Reddy, *Phys. Rev. Lett.* **122**, 122701 (2019), arXiv:1811.12503 [nucl-th].
- [54] J. A. Melendez, C. Drischler, R. J. Furnstahl, A. J. Garcia, and X. Zhang, *J. Phys. G* **49**, 102001 (2022), arXiv:2203.05528 [nucl-th].
- [55] M. Korda and I. Mezić, *Journal of Nonlinear Science* **28**, 687 (2018).
- [56] P. J. Baddoo, B. Herrmann, B. J. McKeon, J. N. Kutz, and S. L. Brunton, “Physics-informed dynamic mode decomposition (pidmd),” (2021), arXiv:2112.04307 [math.DS].
- [57] Q. A. Huhn, M. E. Tano, J. C. Ragusa, and Y. Choi, *Journal of Computational Physics* **475**, 111852 (2023), arXiv:2204.12006 [math.NA].
- [58] M. Velegar, C. Keller, and J. N. Kutz, “Optimized dynamic mode decomposition for reconstruction and forecasting of atmospheric chemistry data,” (2024), arXiv:2404.12396 [cs.LG].
- [59] M. Sharak, A. Safavinejad, and M. Moayyedi, *Journal of Quantitative Spectroscopy and Radiative Transfer* **288**, 108248 (2022).
- [60] M. O. Williams, I. G. Kevrekidis, and C. W. Rowley, *Journal of NonLinear Science* **25**, 1307 (2015), arXiv:1408.4408 [math.DS].
- [61] See Supplemental Material at [URL will be inserted by publisher] for the mathematical formalism pertaining to both the Star Log-extended eMulator (SLM) and parametric extension (pSLM).
- [62] T. Lyons and A. D. McLeod, “Greedy recombination interpolation method (grim),” (2024), arXiv:2205.07495 [math.NA].
- [63] F. Gulminelli and A. R. Raduta, *Phys. Rev. C* **92**, 055803 (2015).
- [64] P.-G. Reinhard, D. J. Dean, W. Nazarewicz, J. Dobaczewski, J. A. Maruhn, and M. R. Strayer, *Phys. Rev. C* **60**, 014316 (1999).
- [65] J. Dobaczewski, H. Flocard, and J. Treiner, *Nuclear Physics A* **422**, 103 (1984).
- [66] Bayesian Analysis of Nuclear Dynamics (BAND) Framework project (2020) <https://bandframework.github.io/>.

Supplemental Material

Sudhanva Lalit ^{1,*} Alexandra C. Semposki ^{2,†} and Joshua M. Maldonado ^{2,‡}

¹Facility for Rare Isotope Beams, Michigan State University, East Lansing, MI 48824, USA

²Department of Physics and Astronomy and Institute of Nuclear and Particle Physics, Ohio University, Athens, OH 45701, USA
(Dated: November 19, 2024)

Supplemental material for the Letter, describing the scaling of the Tolman-Oppenheimer-Volkoff (TOV) equations, including tidal deformability, and the formalism of our Star Log-extended eMulation (SLM) method for both the logarithmic extension and the parametric algorithm.

SCALING TOV AND TIDAL EQUATIONS

The TOV equations [1, 2], along with the tidal deformability equation [3–5], are given by

$$\frac{dp}{dr} = -\frac{G}{c^2}(\epsilon(r) + P(r))\frac{M(r) + 4\pi r^3 P(r)/c^2}{r(r - 2GM(r)/c^2)} \quad (1)$$

$$\frac{dm}{dr} = 4\pi r^2 \frac{\epsilon(r)}{c^2} \quad (2)$$

$$\frac{dy}{dr} = -\frac{y(r)^2}{r} - \frac{F(r)y(r)}{r} - \frac{Q(r)}{r} \quad (3)$$

where,

$$F(r) = \frac{1 - 4\pi Gr^2 (\epsilon(r) - P(r))/c^4}{1 - 2\frac{GM}{rc^2}} \quad (4)$$

and

$$Q(r) = \frac{4\pi Gr^2/c^4}{1 - 2\frac{GM}{rc^2}} \left(5\epsilon(r) + 9p(r) + \frac{\epsilon(r) + p(r)}{c_s(r)^2} c^2 - \frac{6c^4}{4\pi r^2 G} \right) - 4 \left(\frac{G(M(r)/(rc^2) + 4\pi r^2 p(r)/c^4)}{1 - 2GM/(rc^2)} \right)^2 \quad (5)$$

where $y(r) = \frac{R\beta(R)}{H(R)}$ and $\beta = dH/dr$.

Following closely Ref. [6], we use the scaling $r = R_0 x$, $M = M_0 m(x)$, $P = P_0 p(x)$, $\epsilon = \epsilon_0 \epsilon(x)$. To define the relevant scales, we set

$$\epsilon_0 = P_0 \equiv \frac{1}{8\pi^2} \frac{(m_n c^2)^4}{(\hbar c)^3} \approx 1.285 \text{ GeV/fm}^3 \quad (6)$$

and adopt the natural normalization:

$$\left[\frac{2GM_0}{c^2 R_0} \right] = \left[\frac{4\pi R_0^3 \epsilon_0}{3M_0 c^2} \right] = 1 \quad (7)$$

Setting these quantities to unity, meaning to a dimensionless value of order one, establishes “natural” length and mass scales for the problem. This leads to

$$R_0 = \sqrt{\frac{3\pi}{\alpha_G}} \lambda_n \approx 8.378 \text{ km} \quad (8)$$

$$M_0 = \left(\frac{R_0}{R_s^\odot} \right) M_\odot \approx 2.837 M_\odot \quad (9)$$

where α_G is the small, dimensionless gravitational coupling strength between two neutrons (or the neutron mass to Planck mass ratio), λ_n is the neutron’s Compton wavelength, and R_s^\odot represents the Sun’s Schwarzschild radius. Numerically, these values are:

$$\alpha_G = \frac{Gm_n^2}{\hbar c} \approx 5.922 \times 10^{-39} \quad (10)$$

$$\lambda_n = \frac{\hbar c}{m_n c^2} \approx 0.210 \times 10^{-18} \text{ km} \quad (11)$$

$$R_s^\odot = \frac{2GM_\odot}{c^2} \approx 2.953 \text{ km}. \quad (12)$$

The resulting scaled equations are given by

$$\frac{dp}{dx} = -\frac{1}{2} \frac{(\epsilon(x) + p(x)) (m(x) + 3x^3 p(x))}{x^2 (1 - m(x)/x)} \quad (13)$$

$$\frac{dm}{dx} = 3x^2 \epsilon(x) \quad (14)$$

$$\frac{dy}{dx} = -\frac{y(x)^2}{x} - \frac{F(x)y(x)}{x} - \frac{Q(x)}{x} \quad (15)$$

with

$$F(x) = \frac{1 - \frac{3}{2}(\epsilon(x) - p(x))}{1 - \frac{m(x)}{x}},$$

and

$$Q(x) = \frac{\frac{3}{2}x^2}{\left(1 - \frac{m(x)}{x}\right)} \left[5\epsilon(x) + 9p(x) + \frac{\epsilon(x) + p(x)}{c_s^2(x)} - \frac{4}{x^2} \right] - \left(\frac{m(x)/x + 3x^2 p(x)}{\left(1 - \frac{m(x)}{x}\right)} \right)^2.$$

Solving these equations, we get $m(x)$, $p(x)$, $y(x)$ as functions of x . To calculate the mass radius curve of a neutron star, one enforces the boundary condition that the pressure of star is zero at the surface. This enables one to find the mass and radius of the star for a given central pressure.

We use $y_R = y(r = R)$ where R is the radius of the star with mass $M[M_\odot]$ to calculate the compactness of the star $\beta = GM/R$. Using this one can then calculate the dimensionless Love number k_2 as

$$k_2 = \frac{8\beta^5}{5} (1 - 2\beta)^2 [2 + 2\beta(y_R - 1) - y_R]$$

$$\begin{aligned} & \times \{2\beta(6 - 3y_R + 3\beta(5y_R - 8)) \\ & + 4\beta^3 [13 - 11y_R + \beta(3y_R - 2) + 2\beta^2(1 + y_R)] \\ & + 3(1 - 2\beta)^2 [2 - y_R + 2\beta(y_R - 1)] \log(1 - 2\beta)\}^{-1}. \end{aligned} \quad (16)$$

STAR LOG-EXTENDED EMULATION (SLM)

Formalism

Given a possibly nonlinear radial dynamical system

$$\frac{\partial y}{\partial r} = \mathcal{F}(y(\mathbf{x}, r)), \quad (17)$$

where \mathcal{F} is a nonlinear operator that describes the governing equation, one can discretize the phase space to obtain a system of coupled ordinary differential equations (ODEs)

$$\frac{d\mathbf{y}}{dr} = \mathbf{F}(\mathbf{y}(r), r), \quad (18)$$

where $\mathbf{y} \in \mathbb{R}^N$ is a vector representing the state of the radial dynamical system for each of the N degrees of freedom at a given r and $\mathbf{F}(\cdot)$ represents the dynamics in a discrete setting.

Following the DMD formalism, we replace the operator $\mathbf{F}(\cdot)$ of Eq. (18) with a linear operator to capture the evolution of the solution \mathbf{y} . Hence, we seek the following surrogate system

$$\frac{d\mathbf{y}}{dr} = \hat{\mathbf{A}}\mathbf{y}, \quad (19)$$

which, in effect, assumes that the data collected was generated from linear dynamics and that the linear operator $\hat{\mathbf{A}}$ approximates these dynamics. The operator $\hat{\mathbf{A}}$ is learned in a data-driven fashion. We collect a series of snapshots and take the logarithm of the data, i.e., $\log \mathbf{S} = \log[\mathbf{y}_0, \mathbf{y}_1, \dots, \mathbf{y}_m] = \log[\mathbf{y}_i]_{i=0}^m \in \mathbb{R}^{n \times m}$. We then call $\log \mathbf{y}_r$ the *snapshot* of the vector quantity of interest collected at a given position r . We seek an operator $\hat{\mathbf{A}} \in \mathbb{R}^{n \times n}$ such that

$$\log \mathbf{y}_{r+\delta r} = \hat{\mathbf{A}} \log \mathbf{y}_r, \quad (20)$$

where $\log \mathbf{y}_r, \log \mathbf{y}_{r+\delta r}$ are the two snapshots collected in sequential instants. The operator $\hat{\mathbf{A}}$ can be thought of as a finite approximation of the infinite-dimensional *Koopman operator* [7]. Henceforth, we denote $\mathbf{z} = \log \mathbf{y}$ to make notation simpler. We arrange the snapshots in two matrices, $\mathbf{S}^+, \mathbf{S}^- \in \mathbb{R}^{n \times (m-1)}$, defined as

$$\mathbf{S}^- = [\mathbf{z}_0 \ \mathbf{z}_1 \ \dots \ \mathbf{z}_{m-1}], \quad \mathbf{S}^+ = [\mathbf{z}_1 \ \mathbf{z}_2 \ \dots \ \mathbf{z}_m]. \quad (21)$$

The matrix \mathbf{S}^- is called the *lagged matrix of snapshots* and \mathbf{S}^+ is called the *forward matrix of snapshots*. We

now attempt to find the matrix \mathbf{A} such that $\mathbf{S}^+ \approx \mathbf{A}\mathbf{S}^-$. Denoting the Moore-Penrose pseudoinverse operator by \dagger , we can find the best-fit operator $\mathbf{A} = \mathbf{S}^+(\mathbf{S}^-)^\dagger$. However, this computation is expensive, so we follow another path.

We calculate the singular value decomposition (SVD) of $\mathbf{S}^- \approx \mathbf{U}\mathbf{\Sigma}\mathbf{V}^T$, where $\mathbf{U} \in \mathbb{R}^{n \times n}$ and $\mathbf{V}^T \in \mathbb{R}^{m \times m}$ are two orthogonal matrices that hierarchically contain the principal modes of the solutions of the system. The orthogonality of this matrix will be key to ensure that the algorithm will yield the correct modes for the reduced Koopman operator. $\mathbf{\Sigma} \in \mathbb{R}^{n \times m}$ stores the singular values σ_i .

We then reduce the rank by truncating \mathbf{U} and \mathbf{V} to the first r columns, i.e., define $\mathbf{U}_r = [\mathbf{u}]_{i=1}^r \in \mathbb{R}^{n \times r}$ and $\mathbf{V}_r[\mathbf{v}]_{i=1}^r \in \mathbb{R}^{m \times r}$, respectively. We also select the first r singular values in $\mathbf{\Sigma}$ defining a diagonal matrix $\mathbf{\Sigma}_r = \text{diag}([\Sigma]_{i=1}^r) \in \mathbb{R}^{r \times r}$. The rank r is chosen such that a certain fraction of the information is retained, i.e.,

$$r = \text{argmin}_j \frac{\sum_{i=1}^j \sigma_i}{\sum_{i=1}^n \sigma_i}, \tau \quad (22)$$

where τ is a user-specified fraction between 0 and 1. With the truncated SVD, we have

$$\mathbf{S}^- \approx \mathbf{U}_r \mathbf{\Sigma}_r \mathbf{V}_r^T. \quad (23)$$

Then, using the orthogonality of \mathbf{U} and \mathbf{V} and plugging Eq. (23) into Eq. (20), we obtain the reduced Koopman operator in matrix form as

$$\mathbf{A}_r \equiv \mathbf{U}_r^T \mathbf{A} \mathbf{U}_r = \mathbf{U}_r^T \mathbf{S}^+ \mathbf{V}_r \mathbf{\Sigma}_r^{-1}. \quad (24)$$

\mathbf{A}_r is of size $r \times r$, with $r \ll n$; hence, \mathbf{A}_r is a much smaller matrix than \mathbf{A} , making it computationally inexpensive to perform the eigen-decomposition of $\mathbf{A}_r \in \mathbb{R}^{r \times r}$, which yields

$$\mathbf{A}_r \mathbf{W} = \mathbf{\Lambda} \mathbf{W}. \quad (25)$$

The projected modes are then computed as $\Phi = \mathbf{U}_r \mathbf{W}$ and the evolution of the reconstructed system can then be computed via the formula

$$\mathbf{y}(t) = \Phi \mathbf{\Lambda}^{t/\Delta t} \mathbf{b}_0 = \sum_{i=1}^r b_{0i} \phi_i(\lambda_i)^{t/\Delta t}, \quad (26)$$

where $\mathbf{b}_0 = \Phi^\dagger \mathbf{y}_0 \in \mathbb{R}^n$ is the vector of initial coefficients, Φ^\dagger is the pseudo-inverse of the matrix of modes, and $\mathbf{y}_0 \in \mathbb{R}^n$ is the snapshot at the initial time. The full SLM algorithm is given in Alg. 1.

Extended SLM

We integrate machine learning techniques with SLM within the framework of the Koopman operator and its observables [8]. Deriving from support vector machines

Algorithm 1: SLM Algorithm

- 1: Solve Eq. (20) and collect snapshots $[\mathbf{y}_i]_{i=0}^m$ where i are the data indices.
 - 2: Take the log of these snapshots $[\log \mathbf{y}(r_i)]_{i=0}^m$.
 - 3: Extend the snapshots by adding the Hadamard product of the arrays, i.e. $\prod_{i,j} \log \mathbf{y}_i \log \mathbf{y}_j$.
 - 4: Arrange snapshots in \mathbf{S}^+ and \mathbf{S}^- data matrices.
 - 5: Perform SVD of \mathbf{S}^- : $\mathbf{S}^- = \mathbf{U}\mathbf{\Sigma}\mathbf{V}^T$.
 - 6: Retain r modes and compute the reduced Koopman operator $\mathbf{A}_r \equiv \mathbf{U}_r^T \mathbf{A} \mathbf{U}_r = \mathbf{U}_r^T \mathbf{S}^+ \mathbf{V}_r \mathbf{\Sigma}_r^{-1}$.
 - 7: Perform the eigen-decomposition of \mathbf{A}_r to obtain the reduced eigen-modes, $\mathbf{A}_r \mathbf{W} = \mathbf{\Lambda} \mathbf{W}$.
 - 8: Recover the full-state modes $\mathbf{\Phi} = \mathbf{U}_r \mathbf{W}$.
 - 9: Reconstruct the full state solution $\mathbf{y}(r)$, Eq. 20 and exponentiate the solutions.
-

and kernel methods such as radial basis functions, a common choice for constructing the space \mathcal{S} is the set of polynomials

$$S_j(y) = \{y, y^2, y^3, \dots, y^n\}. \quad (27)$$

The objective is to select a sufficiently rich and diverse set of observables, regardless of the specific feature space chosen, to enable an accurate approximation of the Koopman operator. To expand the collection of appropriate observables, a large set of candidate observables is selected with the expectation that a sufficiently diverse set will contain enough features to accurately reconstruct the triplet pair that inherently defines the nonlinear dynamical system being studied [7].

Since Koopman theory allows for a much broader set of observables, we use the set

$$S_j(y) = \{\log y, (\log y)^2\} \quad (28)$$

as the set of polynomials in $\log y$ for extended SLM. This greatly improves the reconstruction and prediction of data. A good observable is guessed by the form of our equation.

Parametric SLM (pSLM)

We expand upon the general algorithm for SLM presented in the previous section, in order to determine the evolution of the system under parametric dependence. The governing equations in Eq. (17) may depend on certain parameters μ and can be reformulated in a parametric form, written as

$$\frac{\partial \mathbf{y}^\mu}{\partial r} = \mathcal{F}(\mathbf{y}^\mu(\mathbf{x}, r; \mu), r; \mu). \quad (29)$$

After discretization of the phase space, one obtains a system of coupled parametric ODEs

$$\frac{d\mathbf{y}^\mu}{dr} = \mathbf{F}(\mathbf{y}^\mu(r; \mu), r; \mu). \quad (30)$$

In parametric SLM, one seeks to replace the operator $\mathbf{F}(\cdot)$ with a linear surrogate

$$\frac{d\mathbf{y}^\theta}{dt} = \hat{\mathbf{A}}(\boldsymbol{\theta}) \mathbf{y}^\theta, \quad (31)$$

where $\boldsymbol{\theta}$ is a vector of parameters corresponding to a prediction set.

In this work we use the reduced Eigen-Pair Interpolation (rEPI) method proposed in [9]. Given a test parameter set $\boldsymbol{\theta}$, we only perform individual classical SLMs for a small dataset. We then use a greedy recombination interpolation method, Banach-GRIM [10], to pick the nearest neighbor of the test parameter $\boldsymbol{\theta}$. Thus we perform a greedy interpolation of the eigen-pairs of the reduced Koopman operator. In this method, we compute SVD decompositions of J data sets and select the largest of the J ranks ($r = \max_{j \in J} (r_j)$), yielding the reduced left- and right-singular matrices \mathbf{U}_{jr} and \mathbf{V}_{jr}^T , as well as the reduced singular value matrix $\mathbf{\Sigma}_{jr}$. We construct the J individual reduced Koopman operators in matrix form

$$\mathbf{A}_{jr} = \mathbf{U}_{jr}^T \mathbf{S}_j^+ \mathbf{V}_{jr} \mathbf{\Sigma}_{jr}^{-1}, \quad (32)$$

from which we obtain the reduced eigen-pairs

$$\mathbf{A}_{jr} \mathbf{W}_{jr} = \mathbf{\Lambda}_{jr} \mathbf{W}_{jr}. \quad (33)$$

The test case eigen-pair of interest ($\mathbf{\Lambda}_{\boldsymbol{\theta}_r}, \mathbf{W}_{\boldsymbol{\theta}_r}$) is obtained via Banach-GRIM, which uses the J eigen-pairs ($\mathbf{\Lambda}_{jr}, \mathbf{W}_{jr}$). We also compute $\mathbf{U}_{\boldsymbol{\theta}_r}$ and \mathbf{b}_θ in the same manner. The projected modes are then calculated using $\mathbf{\Phi}_\theta = \mathbf{U}_{\boldsymbol{\theta}_r} \mathbf{W}_{\boldsymbol{\theta}_r}$. We reconstruct the solutions for the test parameter set $\boldsymbol{\theta}$ using Eq. (26). The corresponding full algorithm for pSLM is given in Alg. 2.

Banach greedy recombination interpolation method

In this method [10], one finds sparse approximations of functions with the aim of reducing computational complexity. The main advantage of this method is its success in higher dimensional spaces where other methods such as Lagrange interpolation fail. The method is divided into two steps: 1) Banach extension and 2) Banach recombination.

Banach Extension

Let $u \in \text{Span}(\mathcal{F})$ and assume $L \subset \Sigma$ be a finite collection of linear functionals. For each choice of subset

Algorithm 2: Parametric SLM via reduced Eigen-Pair Interpolation

▷ Steps 1-7 are offline

1: Solve Eq. (29) for all training parameters $\boldsymbol{\mu}_j$ and collect N_s snapshots $\mathbf{S}_{\boldsymbol{\mu}_j} = [\mathbf{y}(r_i; \boldsymbol{\mu}_j)]_{i=0}^m$ for $1 \leq j \leq N_s$.

2: Take the log of these snapshots $[\log \mathbf{y}(r_i; \boldsymbol{\mu}_j)]_{i=0}^m$.

3: Extend the snapshots by adding the Hadamard product of the arrays, i.e. $\left[\prod_{i,k} \log \mathbf{y}_i \log \mathbf{y}_k \right]_j$, $1 \leq j \leq J$.

4: Arrange snapshots in \mathbf{S}_j^+ and \mathbf{S}_j^- data matrices, $1 \leq j \leq J$.

5: Perform SVD of \mathbf{S}_j^- : $\mathbf{S}_j^- = \mathbf{U}_j \boldsymbol{\Sigma}_j \mathbf{V}_j^T$, $1 \leq j \leq J$.

6: Retain r modes and compute the reduced Koopman operator $\mathbf{A}_{jr} \equiv \mathbf{U}_{jr}^T \mathbf{A} \mathbf{U}_{jr} = \mathbf{U}_{jr}^T \mathbf{S}_j^+ \mathbf{V}_{jr} \boldsymbol{\Sigma}_{jr}^{-1}$, $1 \leq j \leq J$.

7: Perform the eigen-decomposition of \mathbf{A}_{jr} to obtain the reduced eigen-modes, Eq. (29).

▷ Steps 8-11 are online

8: Interpolate SVD-modes \mathbf{U}_j , eigen-modes \mathbf{W}_{jr} , and eigen-values $\boldsymbol{\Lambda}_{jr}$ for to find $\mathbf{U}_{\theta r}$, $\mathbf{W}_{\theta r}$, and $\boldsymbol{\Lambda}_{\theta r}$, respectively.

9: Construct modes $\boldsymbol{\Phi}_\theta = \mathbf{U}_{\theta r} \mathbf{W}_{\theta r}$.

10: Recover the initial coefficients \mathbf{b}_θ by interpolating \mathbf{b}_j , $1 \leq j \leq J$.

11: Reconstruct the full state solution and exponentiate to obtain $\mathbf{y}^\theta(r)$.

$L \subset \Sigma$, we use recombination to find $u \in \text{Span}(\mathcal{F})$ that is an approximation to φ , where φ is the solution one seeks throughout L . In general, this method results in numerical errors. To minimize these, one assumes that $u \in \text{Span}(\mathcal{F})$ is *close* to φ at each functional $\sigma \in L$. This is made precise in the recombination.

Banach recombination

Banach recombination consists of three steps.

1. Let $L_j \subset \Sigma$ be the subset resulting from applying a random permutation to the ordering of elements in L .
2. Apply recombination thinning to find an element $u_j \in \text{Span}(\mathcal{F})$ that satisfies $|\sigma(\varphi - u_j)| \leq \varepsilon_0$ for every $\sigma \in L_j$, where ε_0 is a small number.
3. Finally, we compute $E[u_j] := \max\{|\sigma(\varphi - u_j)| : \sigma \in \Sigma\}$.

After obtaining the elements u_1, \dots, u_s , define u by

$$u := \operatorname{argmin} E[w] : w \in \{u_1, \dots, u_s\}. \quad (34)$$

Then u is our approximation of φ that we seek. The algorithm for the method is provided in Ref. [10].

* lalit@frib.msu.edu

† as727414@ohio.edu

‡ jm998521@ohio.edu

- [1] R. C. Tolman, Static Solutions of Einstein's Field Equations for Spheres of Fluid, *Physical Review* **55**, 364 (1939).
- [2] J. R. Oppenheimer and G. M. Volkoff, On Massive Neutron Cores, *Physical Review* **55**, 374 (1939).
- [3] T. Hinderer, Tidal Love numbers of neutron stars, *Astrophys. J.* **677**, 1216 (2008), [Erratum: *Astrophys. J.* 697, 964 (2009)], arXiv:0711.2420 [astro-ph].
- [4] T. Hinderer, B. D. Lackey, R. N. Lang, and J. S. Read, Tidal deformability of neutron stars with realistic equations of state and their gravitational wave signatures in binary inspiral, *Phys. Rev. D* **81**, 123016 (2010), arXiv:0911.3535 [astro-ph.HE].
- [5] S. Postnikov, M. Prakash, and J. M. Lattimer, Tidal Love Numbers of Neutron and Self-Bound Quark Stars, *Phys. Rev. D* **82**, 024016 (2010), arXiv:1004.5098 [astro-ph.SR].
- [6] J. Piekarewicz, Neutron star matter equation of state, in *Handbook of Supernovae*, edited by A. W. Alsabti and P. Murdin (Springer International Publishing, Cham, 2017) pp. 1075–1094.
- [7] S. L. Brunton, M. Budišić, E. Kaiser, and J. N. Kutz, *Modern koopman theory for dynamical systems* (2021), arXiv:2102.12086 [math.DS].
- [8] J. N. Kutz, S. L. Brunton, B. W. Brunton, and J. L. Proctor, *Dynamic Mode Decomposition* (Society for Industrial and Applied Mathematics, Philadelphia, PA, 2016) <https://epubs.siam.org/doi/pdf/10.1137/1.9781611974508>.
- [9] Q. A. Huhn, M. E. Tano, J. C. Ragusa, and Y. Choi, Parametric dynamic mode decomposition for reduced order modeling, *Journal of Computational Physics* **475**, 111852 (2023), arXiv:2204.12006 [math.NA].
- [10] T. Lyons and A. D. McLeod, Greedy recombination interpolation method (grim) (2024), arXiv:2205.07495 [math.NA].